applied sciences

MDPI

Article

Hybrid Resonant Converter with Three Half-Bridge Legs for Wide Voltage Operation

Bor-Ren Lin * and Yong-Sheng Zhuang

Department of Electrical Engineering, National Yunlin University of Science and Technology, Yunlin 640, Taiwan; M10612005@yuntech.edu.tw

* Correspondence: linbr@yuntech.edu.tw; Tel.: +886-912312281

Received: 13 November 2019; Accepted: 30 December 2019; Published: 31 December 2019

check for updates

Abstract: This paper studied a hybrid resonant converter with three half bridge legs for wide input voltage operation. Compared to the conventional resonant converters with narrow voltage operation, the presented converter can achieve wider voltage operation. On the basis of the proper switching status of power switches, the developed converter can operate at half-bridge resonant circuit under high input voltage range and the other two full-bridge resonant circuits under medium and low input voltage ranges. Each resonant circuit has a 2:1 ($V_{in,max}$ = $2V_{in,min}$) input voltage operation range. Therefore, the developed converter can achieve an 8:1 ($V_{in,max}$ = $8V_{in,min}$) wide voltage operation. The main advantage of the studied converter is the single-stage direct current (DC)/DC power conversion instead of the two-stage power conversion to achieve wide voltage operation. Because the equivalent resonant tank of the adopted converter is controlled by frequency modulation, the soft switching operation on power switches or rectifier diodes can be realized to improve circuit efficiency. The performance of the proposed circuit was confirmed and verified by experiments with a laboratory circuit.

Keywords: DC/DC converters; zero voltage switching; frequency modulation; resonant converters

1. Introduction

Power electronic converters with high efficiency are developed for consumer electronics, battery chargers, telecommunication power units, direct current (DC) nano-grid power conversions, internet of things (IOT) power units, and renewable energy conversions. Soft switching techniques for flyback circuits, full bridge converters, and half bridge converters [1–7] have been developed to improve the converter efficiency and eliminate the switching losses. Phase-shift pulse-width modulation (PSPWM) full bridge converter [1,2] uses the phase angle control between the lagging-leg switches and leading-leg switches to control the load voltage and also achieve soft switching operation. However, the lagging-leg switches are hard switching operation at the light load. The high circulating current loss at low duty cycle case is the other drawback. Soft switching flybacks have been discussed in [3,4] for low power applications. Active clamp converter was discussed in [5] to reduce voltage spike on power switches by using active clamp and switch. However, the rectifier diodes have unbalanced voltage and current stresses on the output side. Resonant converters discussed in [6–8] can achieve low switching losses on power semiconductors. However, the output or input voltage range of the resonant converter is limited due to its low voltage gain of the series resonant circuit characteristics.

For solar *photovoltaic or fuel cell* systems [9–13], the output voltage of a solar panel depends on the geographical location and solar intensity. Therefore, the output voltage range of solar panel is wide variation. Power converters with wide input voltage operation have been discussed and developed in [9–12] for fuel cell and solar power converters with the series or parallel connected structure to extend the input voltage range. Full bridge resonant converter with one alternating current (AC) switch and two isolated transformers was developed in [13] to have a wide voltage operation range ($V_{in,max}$ =

$4V_{in,min}$). However, the control algorithm is much more complicated due to four equivalent sub-circuit topologies. The power converters with wide voltage operation are also demanded for the power units in the outdoor LED lighting systems, battery chargers in electric vehicles, and railway vehicles. Due to the variable parallel or series connection of several LED strings for output lighting system, the power converters with variable output voltage are normally implemented. For railway low power supplies, the input voltages of DC converters are between 24 and 110 V for the braking system, electric door system, lighting system, and motor drive controller. For electric vehicle (EV) systems, the output voltage of battery charger is variable from 210 to 450 V. Therefore, DC converters with wide voltage range output is required for EV applications. To achieve wide voltage range output, the two-stage DC converters [14–16] based on the non-isolated DC/DC converter in the first-stage and the isolated DC converter in the second-stage are the simplest way to accomplish wide voltage operation. The main disadvantage of the two-stage converters is low circuit efficiency. Parallel- or series-connected converters [9,17] were developed to have wide voltage operations. However, a large number of circuit components are needed in these circuit topologies. Series resonant converters published in [18–21] have a wide voltage range operation such as $V_{in,max} = 4V_{in,min}$ or $V_{o,max} = 4V_{o,min}$. By the proper control of power switches, the resonant converter can be operated at the half or full bridge circuit topology. Therefore, the resonant converters with 4:1, that is, $V_{in,max} = 4V_{in,min}$, wide voltage range operation are achieved. However, the voltage operation range of these circuit topologies is less than 4, that is, $V_{in,max} \leq 4V_{in,min}$. If the much wider voltage range is requested, such as $V_{in,max} \geq 4V_{in,min}$ in solar panel applications or wide voltage variation systems, then these circuit topologies cannot be operated well.

A new resonant converter with a three converter legs structure and a variable turns ratio of transformer is presented in this study, having a wide voltage range operation. On the basis of the switching status of active switches, the proposed resonant converter has three equivalent sub-circuits to implement 8:1 ($V_{in,max} = 8V_{in,min}$) wide voltage range operation such as 50–400 V. If V_{in} (input voltage) is under low voltage range from 50 to 100 V, the sub-circuit with the full bridge circuit topology and low turns ratio transformer is operated to have high voltage gain. If V_{in} is under medium voltage range from 100 to 200 V, then the sub-circuit with full bridge circuit topology and high turns ratio transformer is operated to decrease the voltage gain in order to control the load voltage. If V_{in} is under the high voltage range from 200 to 400 V, then the sub-circuit with the half bridge circuit topology and high turns ratio is operated to further reduce the voltage gain. Three equivalent sub-circuits in the proposed converter were selected by two Schmitt voltage comparators with reference input voltages at 100 and 200 V. Therefore, the half bridge circuit topology or full-bridge circuit topology with two different turns ratios can be selected on the input side to accomplish wide input voltage operation. The circuit topology and control algorithm of the presented converter are easy to implement when compared to the conventional wide voltage range converters with two-stage circuit topologies and hybrid converters in [9–21]. Because the resonant circuit of the presented DC converter is controlled under the frequency modulation and the input impedance of resonant tank is always at the inductive load operation, active switches are naturally turned on at zero voltage switching operation. Finally, the design procedures and experiments are presented and confirmed with a 480 W laboratory circuit.

2. Circuit Structure and Principle of Operation

The circuit schematic of the developed circuit topology with wide voltage operation is shown in Figure 1. Three half-bridge legs (Q_1–Q_6) are used on the input side and one center-taped rectifier is used on the output side. Two resonant circuits (L_{r1}, C_{r1}, L_{r2} and C_{r2}) with one AC power switch S are used to accomplish series resonant operation with soft switching behavior for power switches. V_{in} (V_o) is the input (output) voltage and R_o is the output resistor. Transformer T has two primary and secondary winding sets with n_p and n_s winding turns, respectively. According to the switching states of Q_1–Q_6 and S, the developed converter can be operated under three input voltage ranges: $V_{in,L} = V_{in,max}/8$–$V_{in,max}/4$, $V_{in,M} = V_{in,max}/4$–$V_{in,max}/2$ and $V_{in,H} = V_{in,max}/2$–$V_{in,max}$, as shown in Figure 2. Figure 2a gives the equivalent resonant circuit if V_{in} is under the low voltage range $V_{in,L}$. To achieve the higher voltage gain in the proposed converter, Q_5, Q_6, and S are off. Only a full-bridge converter with Q_1–Q_4, L_{r1}, C_{r1}, and T with n_p primary turns are operated on the input-side. The DC voltage gain of the resonant circuit in Figure 2a is $V_o/V_{in,L} = G_L(f)n_s/n_p$, where $G_L(f)$ is the voltage gain of the proposed converter in Figure 2a. Figure 2b illustrates the equivalent circuit if V_{in} is under the medium voltage range $V_{in,M}$. In the medium voltage range, Q_3 and Q_4 are off. The resonant tank includes L_{r1}, C_{r1}, L_{r2}, C_{r2}, and transformer T with $2n_p$ primary winding turns. The series resonant frequency of this equivalent circuit is also $f_r = 1/2\pi\sqrt{L_{r1}C_{r1}}$ due to $C_{r1} = C_{r2}$ and $L_{r1} = L_{r2}$. The DC voltage gain of the resonant circuit shown in Figure 2b is $V_o/V_{in,M} = G_M(f)n_s/(2n_p)$ due to the primary turns being $2n_p$ instead of n_p, where $G_M(f)$ is the voltage gain of the proposed converter in Figure 2b. Figure 2c provides the equivalent circuit if V_{in} is under the high voltage range $V_{in,H}$. In high voltage range, Q_3, Q_4, and Q_5 are off and S and Q_6 are on. The half-bridge resonant converter with the components Q_1, Q_2, L_{r1}, C_{r1}, L_{r2}, C_{r2}, and transformer T with $2n_p$ primary winding turns is operated to achieve lower voltage gain. The series resonant frequency of this equivalent circuit is $f_r = 1/2\pi\sqrt{L_{r1}C_{r1}}$ with $L_{r1} = L_{r2}$ and $C_{r1} = C_{r2}$. Compared to the equivalent circuit in Figure 2b, the fundamental input voltage is $V_{in}/2$ in Figure 2c instead of V_{in} in Figure 2b. The DC voltage gain of the equivalent circuit in Figure 2c is $V_o/V_{in,H} = G_H(f)n_s/(4n_p)$, where $G_H(f)$ is the voltage gain of the proposed converter in Figure 2c. Compared to the DC voltage gain under three different input voltage gains, it observes that $V_o/V_{in,L} = 2(V_o/V_{in,M}) = 4(V_o/V_{in,H})$ if $G_L(f) = G_M(f) = G_H(f)$. Thus, the voltage gain of resonant circuit in Figure 2a is the largest compared to the resonant circuits in Figure 2b,c. Power switches Q_1–Q_6 and S can be properly controlled from three equivalent circuits, as shown in Figure 2 to have 8:1 ($V_{in,max} = 8V_{in,min}$) wide voltage range operation.

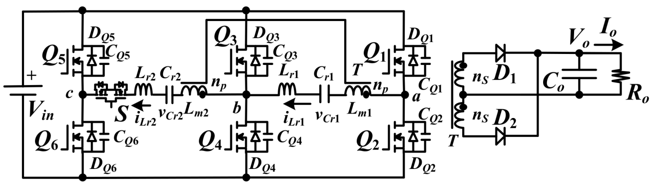

Figure 1. Circuit schematic of the developed converter.

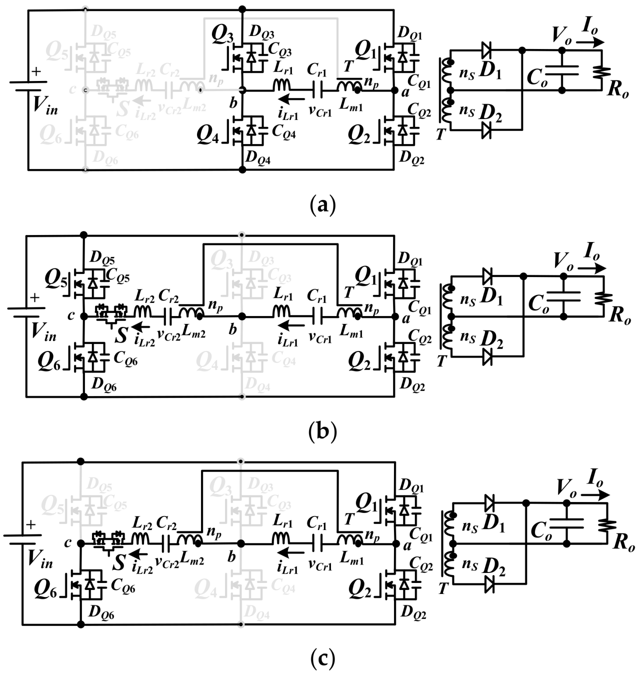

(**a**)

(**b**)

(**c**)

Figure 2. Circuit diagrams for different input voltage ranges: (**a**) low input voltage ($V_{in,L} = V_{in,max}/8$–$V_{in,max}/4$); (**b**) medium input voltage ($V_{in,M} = V_{in,max}/4$–$V_{in,max}/2$); (**c**) high input voltage ($V_{in,H} = V_{in,max}/2$–$V_{in,max}$).

2.1. Low Input Voltage Range (S, Q_5, and Q_6 off, $V_{in,L}$ = $V_{in,max}$/8–$V_{in,max}$/4)

If the input voltage V_{in} is between $V_{in,max}$/8 and $V_{in,max}$/4, S, Q_5, and Q_6 are turned off and only Q_1–Q_4 are operated to realize the high voltage gain shown in Figure 2a compared to the other two equivalent circuits (Figure 2b,c). The input-side is a full-bridge resonant converter and the output-side is a center-tapped diode rectifier. The DC voltage gain for low input voltage range is $V_o/V_{in,L}$ = $G_L(f)n_s/n_p$. The theoretical pulse-width modulation (PWM) waveforms and the equivalent circuits for six operating states are provided in Figure 3 if f_{sw} (switching frequency) is less than f_r (series resonant frequency).

State 1 [t_0–t_1]: At $t = t_0$, $v_{CQ1} = v_{CQ4} = 0$. Then D_{Q1} and D_{Q4} are conducting due to $i_{Lr1}(t_0) < 0$. Q_1 and Q_4 turn on after t_0 to have soft switching operation. In this time interval, L_r and C_r are naturally resonant to deliver power to the load side. Because the diode D_1 is conducting, the magnetizing voltage $v_{Lm1} = nV_o$, where $n = n_p/n_s$, and i_{Lm1} increases.

State 2 [t_1–t_2]: If $f_{sw} < f_r$, then i_{D1} decreases to zero at time t_1 and D_1 is reverse biased without the reverse recovery current. In this state, L_{r1}, L_{m1}, and C_{r1} are naturally resonant with the resonant frequency $f_p = 1/2\pi\sqrt{(L_{r1}+L_{m1})C_{r1}}$.

State 3 [t_2–t_3]: At time t_2, Q_1 and Q_4 turn off. C_{Q1} (C_{Q2}) and C_{Q4} (C_{Q3}) are charged (discharged) due to $i_{Lr1}(t_2)$ being positive. In this state, D_2 is forward biased due to $i_{Lr1} < i_{Lm1}$ and the magnetizing voltage v_{Lm1} equals $-nV_o$.

State 4 [t_3–t_4]: At time t_3, $v_{CQ2} = v_{CQ3} = 0$. D_{Q2} and D_{Q3} are conducting owing to $i_{Lr1}(t_3) > 0$. Q_2 and Q_3 turn on after t_3 to realize the soft switching operation. In this time interval, L_r and C_r are naturally resonant to deliver power to load side. Because the diode D_2 is forward biased on the secondary side, the magnetizing voltage $v_{Lm1} = -nV_o$ and i_{Lm1} decreases.

State 5 [t_4–t_5]: At time t_4, i_{D2} is decreased to zero so that D_2 is off. In this state, L_{r1}, L_{m1}, and C_{r1} are naturally resonant.

State 6 [t_5–T_{sw} + t_0]: At time t_5, power switches Q_2 and Q_3 are turned off. C_{Q1} (C_{Q2}) and C_{Q4} (C_{Q3}) are discharged (charged) due to $i_{Lr1}(t_5)$ is negative. In this state, D_1 is forward biased owing to $i_{Lr1} > i_{Lm1}$ and the magnetizing voltage $v_{Lm1} = nV_o$ and i_{Lm1} increases. At $T_{sw} + t_0$, $v_{CQ1} = v_{CQ4} = 0$ and the converter goes to state 1 for the next switching period.

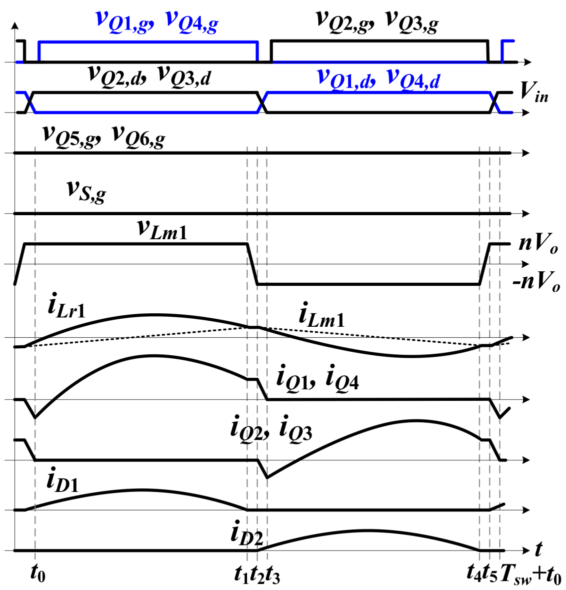

(**a**)

Figure 3. *Cont.*

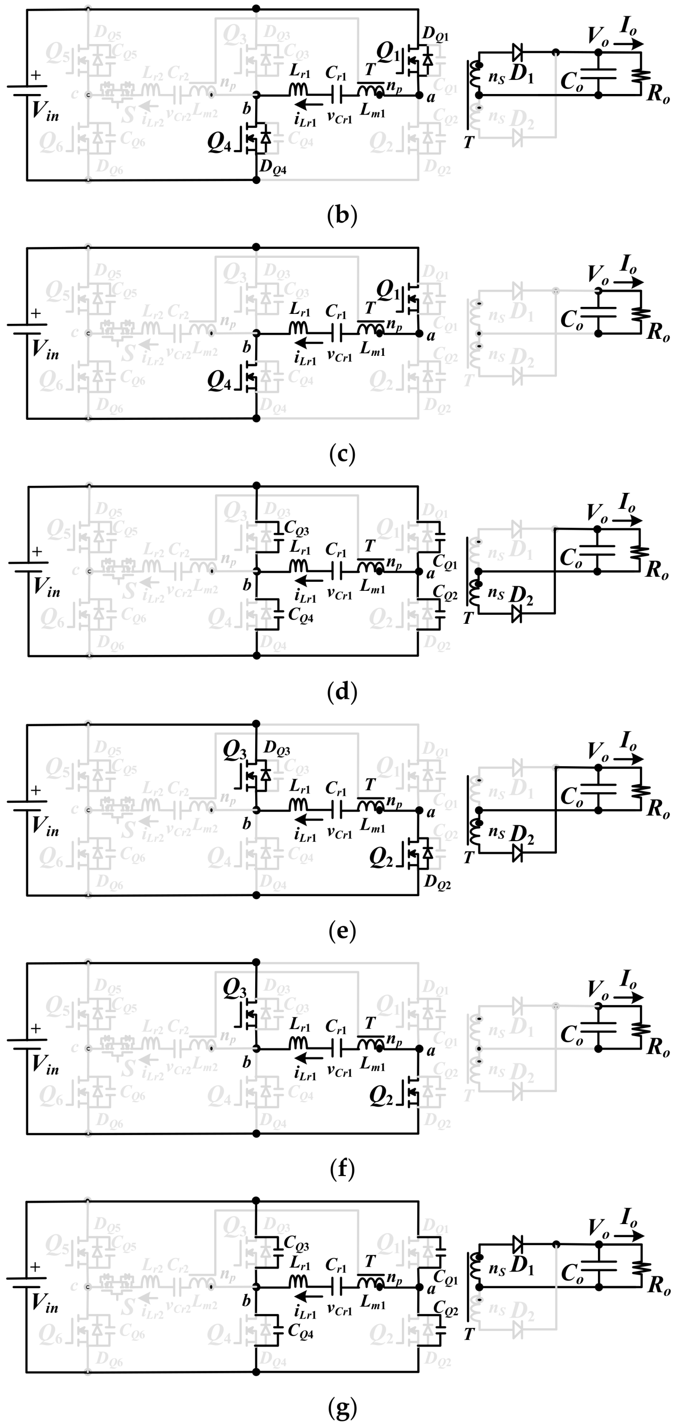

Figure 3. Proposed direct current (DC) converter under low input voltage range: (**a**) pulse-width modulation (PWM) waveforms; (**b**) state 1; (**c**) state 2; (**d**) state 3; (**e**) state 4; (**f**) state 5; (**g**) state 6.

2.2. Medium Input Voltage Range (Q_3 and Q_4 off, $V_{in,M} = V_{in,max}/4$–$V_{in,max}/2$)

The proposed converter for the medium input voltage ($V_{in} = V_{in,max}/4$–$V_{in,max}/2$) operation is illustrated in Figure 2b. Under the medium voltage range, power switches Q_3 and Q_4 turn off and AC switch S is always on. The full-bridge resonant circuit is adopted on the input-side with the resonant components L_{r1}, L_{r2}, C_{r1}, C_{r2}, and transformer T with $2n_p$ primary winding turns. Because $C_{r1} = C_{r2}$ and $L_{r1} = L_{r2}$, the series resonant frequencies at the medium input voltage operation (Figure 2b) and the low input voltage operation (Figure 2a) are identical. The DC voltage gain for the medium voltage range is $V_o/V_{in,M}$ = $G_M(f)n_s/(2n_p)$. Comparing the DC voltage gains for low and medium voltage ranges, one can observe that $V_o/V_{in,L}$ = $2(V_o/V_{in,M})$ under $G_L(f)$ = $G_M(f)$. This means the proposed converter has less DC voltage gain at the medium input voltage range operation. The theoretical PWM waveforms and the equivalent circuits are given in Figure 4.

State 1 [t_0–t_1]: At time t_0, the capacitor voltages of v_{CQ1} and v_{CQ6} are zero. D_{Q1} and D_{Q6} are forward biased due to $i_{Lr1}(t_0)$ being negative. Q_1 and Q_6 can turn on after t_0 to achieve zero-voltage switching. In this state, C_{r1}, C_{r2}, L_{r1}, and L_{r2} are naturally resonant with series resonant frequency $f_r = 1/2\pi\sqrt{L_{r1}C_{r1}}$ due to L_{r1} = L_{r2} and C_{r1} = C_{r2}, and the energy is transferred from V_{in} to R_o. Due to D_1 being forward biased, the magnetizing voltage v_{Lm1} = v_{Lm2} = $(n_p/n_s)V_o$ and i_{Lm1} and i_{Lm2} increase.

State 2 [t_1–t_2]: If f_{sw} (the switching frequency) < f_r (series resonant frequency), then i_{Lm1} = i_{Lr1} and i_{Lm2} = i_{Lr2} at t = t_1. Thus, D_1 is off without reverse recovery current loss. In this state, the circuit components C_{r1}, L_{r1}, C_{r2}, L_{r2}, L_{m1}, and L_{m2} are naturally resonant.

State 3 [t_2–t_3]: Power switches Q_1 and Q_6 turn off at t = t_2. C_{Q1} and C_{Q6} are charged and C_{Q2} and C_{Q5} are discharged due to $i_{Lr1}(t_2) > 0$. Because $i_{Lr1} < i_{Lm1}$ after t_2, the diode D_2 is forward biased.

State 4 [t_3–t_4]:v_{CQ2} and v_{CQ5} are decreased to zero at t = t_3. Because $i_{Lr1}(t_3) > 0$, the body diodes D_{Q2} and D_{Q5} are conducting. Q_2 and Q_5 can be turned on after t_3 to have zero-voltage switching. In this state, C_{r1}, L_{r1}, C_{r2}, and L_{r2} are naturally resonant with series resonant frequency $f_r = 1/2\pi\sqrt{L_{r1}C_{r1}}$ and the energy is transferred from V_{in} to R_o. Due to D_2 being forward biased, the magnetizing voltage v_{Lm1} = v_{Lm2} = $-(n_p/n_s)V_o$ and i_{Lm1} and i_{Lm2} decrease in state 4.

State 5 [t_4–t_5]: At time t_4, i_{Lm1} equals i_{Lr1} and i_{Lm2} equals i_{Lr2}. Therefore, D_2 becomes off. Hence, the components L_{r1}, L_{r2}, C_{r1}, C_{r2} L_{m1}, and L_{m2} are naturally resonant.

State 6 [t_5–T_{sw} + t_0]: Power switches Q_2 and Q_5 are turned off at t = t_5. C_{Q1} (C_{Q2}) and C_{Q6} (C_{Q5}) are discharged (charged) due to $i_{Lr1}(t_5) < 0$. Because $i_{Lr1}(t_5)$ is greater than $i_{Lm1}(t_5)$, the diode D_1 is forward biased. At t = T_{sw}+t_0, v_{CQ1} = v_{CQ6} = 0.

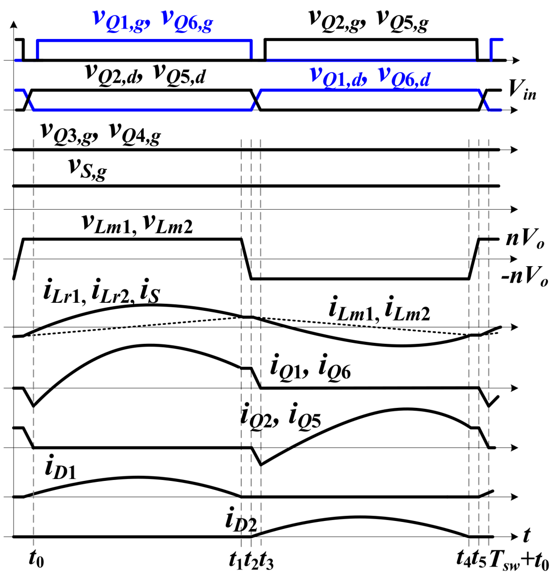

(**a**)

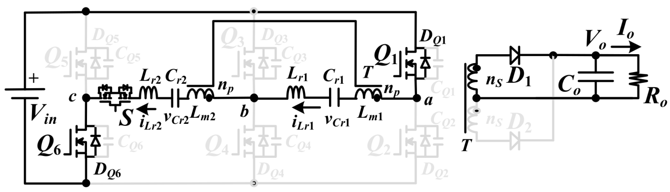

(**b**)

Figure 4. *Cont.*

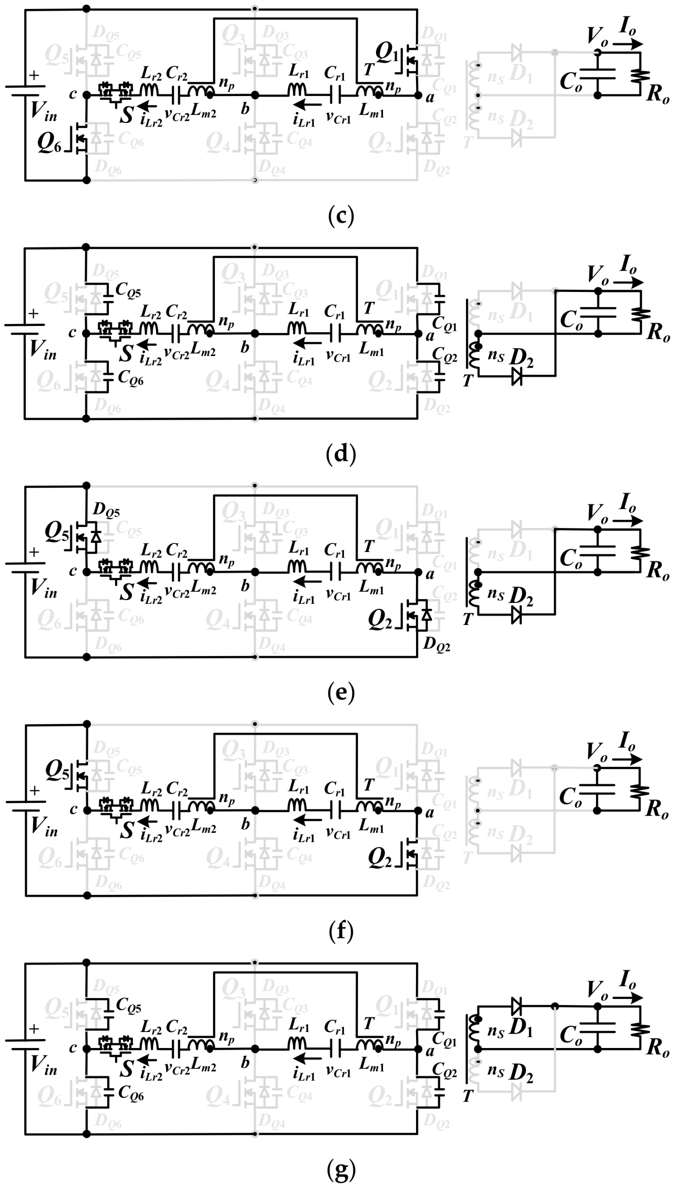

Figure 4. Proposed DC converter under medium input voltage range: (**a**) PWM waveforms; (**b**) state 1; (**c**) state 2; (**d**) state 3; (**e**) state 4; (**f**) state 5; (**g**) state 6.

2.3. High Input Voltage Range (Q_3–Q_4 off, $V_{in,H}$ = $V_{in,max}$/2–$V_{in,max}$)

Figure 2c shows the sub-circuit when V_{in} is in the high voltage range ($V_{in,max}$/2–$V_{in,max}$). Power switches Q_3–Q_5 are turned off, and S and Q_6 are always on. The half-bridge resonant circuit with the components L_{r1}, L_{r2}, C_{r1}, C_{r2}, and transformer T with $2n_p$ primary winding turns is operated to regulate the load voltage. Because C_{r1} = C_{r2} and L_{r1} = L_{r2}, the series resonant frequencies for three input voltage ranges in Figure 2 are identical. The DC voltage gain in the high input voltage range is $V_o/V_{in,H} = G_H(f)n_s/(4n_p)$. Comparing the DC voltage gains for three different input voltage ranges, it is observable that $V_o/V_{in,L} = 2(V_o/V_{in,M}) = 4(V_o/V_{in,H})$ if $G_L(f) = G_M(f) = G_H(f)$. The theoretical PWM waveforms and the equivalent circuits in a switching cycle for high input voltage range are shown in Figure 5.

State 1 [t_0–t_1]: C_{Q1} is discharged to zero voltage at t = t_0. Due to $i_{Lr1}(t_0)$ being negative, the body diode D_{Q1} is forward. Q_1 can turn on after t_0 to realize zero-voltage switching. Because $i_{Lr1}(t_0) > i_{Lm1}$, D_1 is conducting and $v_{Lm1} = v_{Lm2} = nV_o$ and i_{Lm1} and i_{Lm2} increase. C_{r1}, C_{r2}, L_{r1} and L_{r2}, are resonant with resonant frequency $f_r = 1/2\pi\sqrt{L_{r1}C_{r1}}$ in this state.

State 2 [t_1–t_2]: At time t_1, $i_{Lr1} = i_{Lm1}$ and $i_{Lr2} = i_{Lm2}$. The rectifier diode D_1 becomes off. L_{m1}, L_{m2}, L_{r1}, L_{r2}, C_{r1}, and C_{r2} are resonant in this state.

State 3 [t_2–t_3]: Q_1 is turned off at $t = t_2$. Due to i_{Lr1} being positive, C_{Q1} (C_{Q2}) is charged (discharged). The rectifier diode D_2 is forward biased due to $i_{Lr1}(t_2) < i_{Lm1}(t_2)$.

State 4 [t_3–t_4]: $v_{CQ2} = 0$ at $t = t_3$. Owing to $i_{Lr1}(t_3)$ being positive, the body diode D_{Q2} is forward. Power switch Q_2 can turn on after t_3 to achieve zero-voltage switching. D_2 is conducting owing to $i_{Lr1}(t_3) < i_{Lm1}(t_3)$. Thus, $v_{Lm1} = v_{Lm2} = -nV_o$ and i_{Lm1} and i_{Lm2} decrease. C_{r1}, C_{r2}, L_{r1}, and L_{r2} are resonant in this state.

State 5 [t_4–t_5]: At $t = t_4$, i_{Lr1} equals i_{Lm1} and i_{Lr2} equals i_{Lm2}. Then, the rectifier diode D_2 becomes off. In this time interval, L_{m1}, L_{m2}, L_{r1}, L_{r2}, C_{r1}, and C_{r2} are resonant.

State 6 [t_5–T_{sw} + t_0]: Q_2 turns off at t_5. Because i_{Lr1} is negative, C_{Q1} is discharged and C_{Q2} is charged. Due to $i_{Lr1}(t_5) > i_{Lm1}(t_5)$, the rectifier diode D_1 is forward biased. At time $T_{sw} + t_0$, C_{Q1} is discharged to zero voltage.

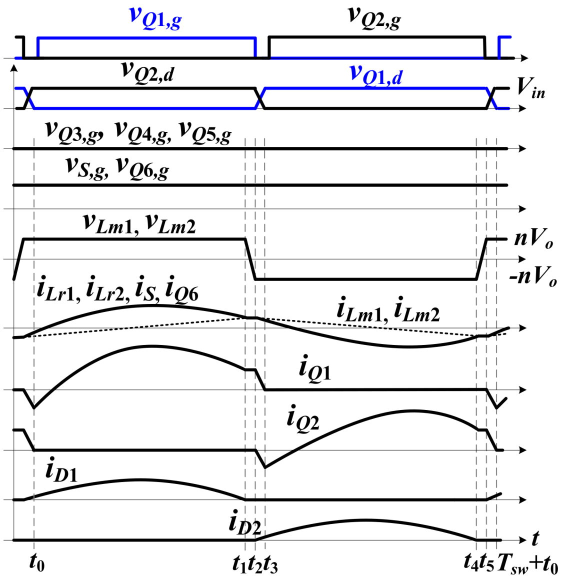

(**a**)

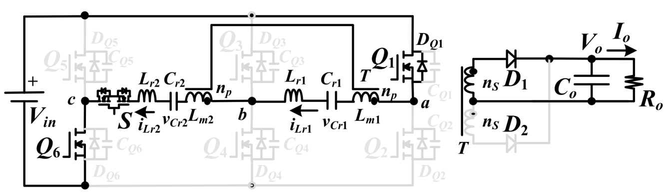

(**b**)

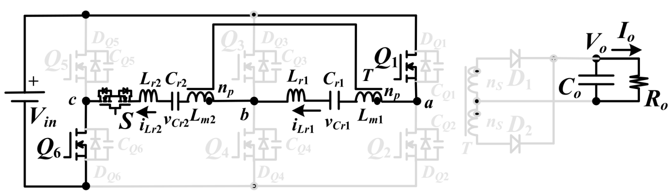

(**c**)

Figure 5. *Cont.*

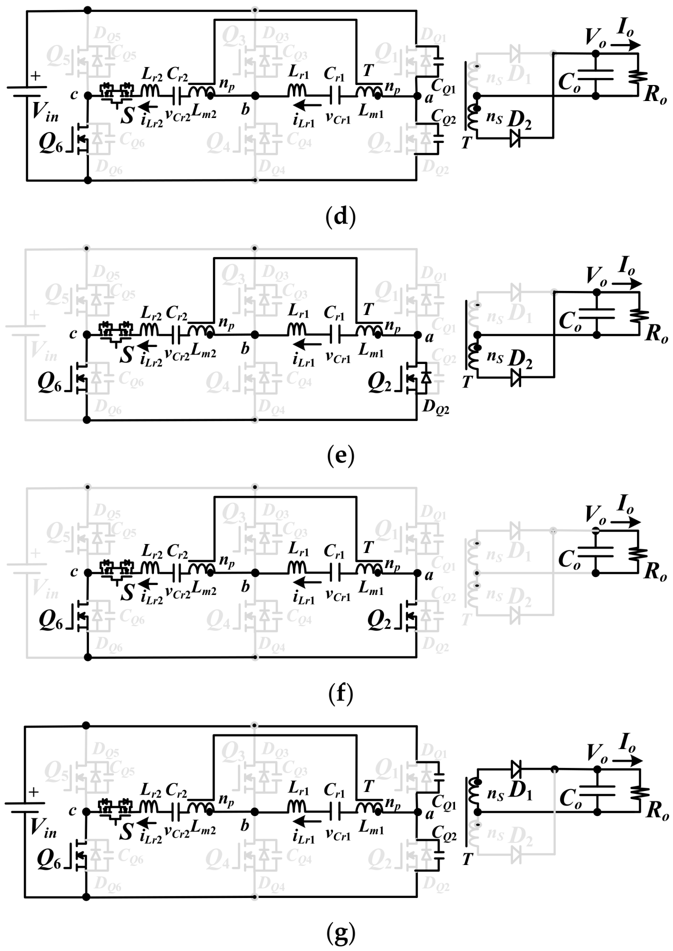

(**d**) (**e**) (**f**) (**g**)

Figure 5. Proposed DC converter under high input voltage range: (**a**) PWM waveforms; (**b**) state 1; (**c**) state 2; (**d**) state 3; (**e**) state 4; (**f**) state 5; (**g**) state 6.

3. Circuit Characteristics

The presented circuit is controlled by frequency modulation. The input voltage V_{in} has a variation between 50 and 400 V and the output voltage V_o is regulated at 48 V. The fundamental harmonic analysis (FHA) proposed by [22] is selected to calculate the voltage transfer function in the proposed converter by frequency modulation. When 50 V ≤ V_{in} < 100 V (low voltage range), only Q_1–Q_4 are operated (Figure 2a) to achieve high voltage gain. The square voltage waveform with voltage values of $\pm V_{in}$ is obtained on the leg voltage v_{ab}. If 100 V ≤ V_{in} < 200 V (medium voltage range), then only power switches Q_1, Q_2, Q_5, and Q_6 are controlled to control load voltage, and AC switch S is always on (Figure 2b). The square waveform with voltage values of $\pm V_{in}$ is obtained on the leg voltage v_{ac}. If 200 V ≤ V_{in} ≤ 400 V (high voltage range), then only Q_1 and Q_2 are operated to control the load voltage, and switches S and Q_6 are always on (Figure 2c). The square waveform with voltage values of 0 and V_{in} is obtained on the leg voltage v_{ac}. The fundamental root mean square (*rms*) values of the leg voltages $v_{ab,rms}$ (in the low voltage range) and $v_{ac,rms}$ (in the medium and high voltage ranges) are calculated as:

$$v_{ab,rms} = 2\sqrt{2}V_{in},\ 50\ V \ \leq V_{in} < 100\ V, \quad (1)$$

$$v_{ac,rms} = \begin{cases} 2\sqrt{2}V_{in},\ 100\ V \ \leq V_{in} < 200\ V \\ \sqrt{2}V_{in},\ 200\ V \ \leq V_{in} < 400\ V \end{cases}. \quad (2)$$

The turns ratio of transformer T under low input voltage range is $n_1 = n_p/n_s$. However, the turn-ratio of transformer T under medium and high input voltage ranges is $n_2 = 2n_p/n_s = 2n_1$. The fundamental *rms* magnetizing voltage $v_{Lm,rms}$ under different input voltage ranges is expressed as

$$v_{Lm,rms} = \begin{cases} 2\sqrt{2}n_1V_o, & 50\ V \leq V_{in} < 100\ V \\ 2\sqrt{2}n_2V_o = 4\sqrt{2}n_1V_o, & 100\ V \leq V_{in} < 400\ V. \end{cases} \quad (3)$$

The relationship between the AC equivalent resistor R_{eq} on the input-side and the DC load resistor R_o is obtained in Equation (4):

$$R_{eq} = \begin{cases} \frac{8n_1^2R_o}{\pi^2}, & 50\ V \leq V_{in} < 100\ V \\ \frac{8n_2^2R_o}{\pi^2} = \frac{32n_1^2R_o}{\pi^2}, & 100\ V \leq V_{in} < 400\ V. \end{cases} \quad (4)$$

Figure 6 shows the corresponding resonant tank of the presented circuit. The voltage transfer function of the corresponding resonant tank is derived and expressed in Equation (5):

$$|G_{ac}| = \frac{v_{out,LLC}}{v_{in,LLC}} = 1/\sqrt{\left[1 + \frac{f_n^2 - 1}{l_n f_n^2}\right]^2 + x^2\left(f_n - \frac{1}{f_n}\right)^2} = \begin{cases} \frac{n_1V_o}{V_{in}}, & 50\ V \leq V_{in} < 100\ V \\ \frac{2n_1V_o}{V_{in}}, & 100\ V \leq V_{in} < 200\ V \\ \frac{4n_1V_o}{V_{in}}, & 200\ V \leq V_{in} < 400\ V, \end{cases} \quad (5)$$

where $x = \sqrt{\left(L_{r,eq}/C_{r,eq}\right)}/R_{eq}$ is the quality factor where $L_{r,eq} = L_{r1}$ and $C_{r,eq} = C_{r1}$ for low input voltage range and $L_{r,eq} = L_{r1} + L_{r2} = 2L_{r1}$ and $C_{r,eq} = C_{r1} \times C_{r2} / (C_{r1} + C_{r2}) = C_{r1}/2$ for medium and high input voltage ranges; $f_n = f_{sw}/f_r$ is the frequency ratio, and $l_n = L_{m,eq}/L_{r,eq}$ is the inductor ratio. According to Equation (5), the DC load voltage V_o can be further rewritten as

$$V_o = V_{in}/m\sqrt{\left[1 + \frac{f_n^2 - 1}{l_n f_n^2}\right]^2 + x^2\left(f_n - \frac{1}{f_n}\right)^2}, \quad (6)$$

where $m = n_1$, if 50 V $\leq V_{in} <$ 100 V; $2n_1$, if 100 V $\leq V_{in} <$ 200 V; or $4n_1$, if 200 V $\leq V_{in} <$ 400 V. On the basis of the actual input voltage value, the switching states of Q_1–Q_6 and S can be properly controlled. From Equation (6), the developed circuit has high voltage gain under low input voltage range. On the other hand, the converter has low voltage gain under high input voltage range.

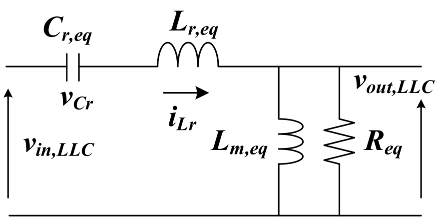

Figure 6. Equivalent circuit of the resonant tank.

4. Design Procedures and Test Results

The design procedures and test results of the presented circuit are verified in this section. A laboratory circuit was built and the electric specifications were V_{in} = 50–400 V, V_o = 48 V, and $I_{o,max}$ = 10 A. The series resonant frequency was designed at 150 kHz. Due to $L_{r1} = L_{r2}$ and $C_{r1} = C_{r2}$, the series resonant frequencies for all three equivalent circuits shown in Figure 2 were identical and designed at 150 kHz. According to the voltage transfer function in Equation (5), the gain curves of the developed resonant converter with different input voltage ranges are given in Figure 7. The transition voltage $V_{in,tran\,1}$ between the low and medium input voltage ranges was designed at 100 V with ±5 V voltage tolerance. Similarly, the transition voltage $V_{in,tran\,2}$ between the medium and high input voltage ranges was designed at 200 V with ±5 V voltage tolerance. From Equation (6), one can observe that the voltage gain at the high input voltage range was about two (four) times of the voltage gain at the medium (low) input voltage range. The design procedures for three equivalent resonant circuits were almost identical. Therefore, the prototype circuit was designed at the low input voltage range to simplify the design consideration. The minimum voltage gain $G_{ac,min}$ at the series resonant frequency was designed as unity and the transition voltage $V_{in,trans\,1}$ = 100 V. The turns ratio $n_1 = n_p/n_s$ can be calculated from Equation (5) and expressed in Equation (7):

$$n_1 = G_{ac,min} \times V_{in,tran\,1} / V_o = 1 \times 100/48 \approx 2.08. \quad (7)$$

Transformer T is implemented by the TDK (Tokyo Electric Chemical Industry Co., Ltd., Tokyo, Japan) magnetic core with ΔB = 0.4 *tesla* and A_e = 354 mm^2. The series resonant frequency was selected at 150 kHz. The primary turns of transformer are obtained in Equation (8):

$$n_{p,min} > n_1 V_o / [f_{sw} \Delta B A_e] = 2.08 \times 48 / [150000 \times 0.4 \times 0.000354] \approx 4.7. \quad (8)$$

The actual primary turns and secondary turns in the prototype circuit were n_p = 8 and n_s = 4. The equivalent resistance R_{eq} at the rated power is given in Equation (9):

$$R_{eq} = 8 n_1^2 R_o / \pi^2 = 8 \times 2^2 \times (48/10)/3.14159^2 = 15.56\ \Omega. \quad (9)$$

The inductor ratio $l_n = L_{m1}/L_{r1}$ = 3 and quality factor x = 0.25 were selected in the prototype circuit. L_{r1} and L_{r2} are obtained from Equation (10) and C_{r1} and C_{r2} are calculated in Equation (11):

$$L_{r1} = L_{r2} = \frac{x R_{eq}}{[2\pi f_r]} = 4.13\ \mu\text{H}, \quad (10)$$

$$C_{r1} = C_{r2} = \frac{1}{4\pi^2 L_{r1} f_r^2} \approx 273\ \text{nF}. \quad (11)$$

The magnetizing inductors L_{m1} and L_{m2} are expressed in Equation (12):

$$L_{m1} = L_{m2} = l_n \times L_{r1} \approx 12.4\ \mu\text{H}. \quad (12)$$

The voltage stress of power MOSFETs (metal–oxide–semiconductor field-effect transistor) Q_1–Q_6 and switch S was the maximum input voltage $V_{in,max}$ = 400 V. The theoretical voltage ratings of the rectifier diodes D_1 and D_2 were $2V_o$ = 98 V. Figure 8 shows the control block of the signals Q_1–Q_6 and S. Two Schmitt trigger comparators were used for transition voltages 100 and 200 V to select the correct range of input voltage. Figure 9 and Table 1 give the photographs and all circuit components used in the prototype circuit, respectively. Figure 9a shows the photograph of the prototype circuit. The control board for selecting the correct range of input voltage and the consequent bridge configuration is given in Figure 9b. The experimental setup, including the test equipment, is provided in Figure 9c. The list of equipment that was used to record the results is as follows: Chroma 62012P-600-8 (DC voltage source), Chroma 63112A (DC electronic load), TCP302 and TCP312 (current probe), TDS3014 (digital oscilloscope), and SI-9110 (isolated voltage probe).

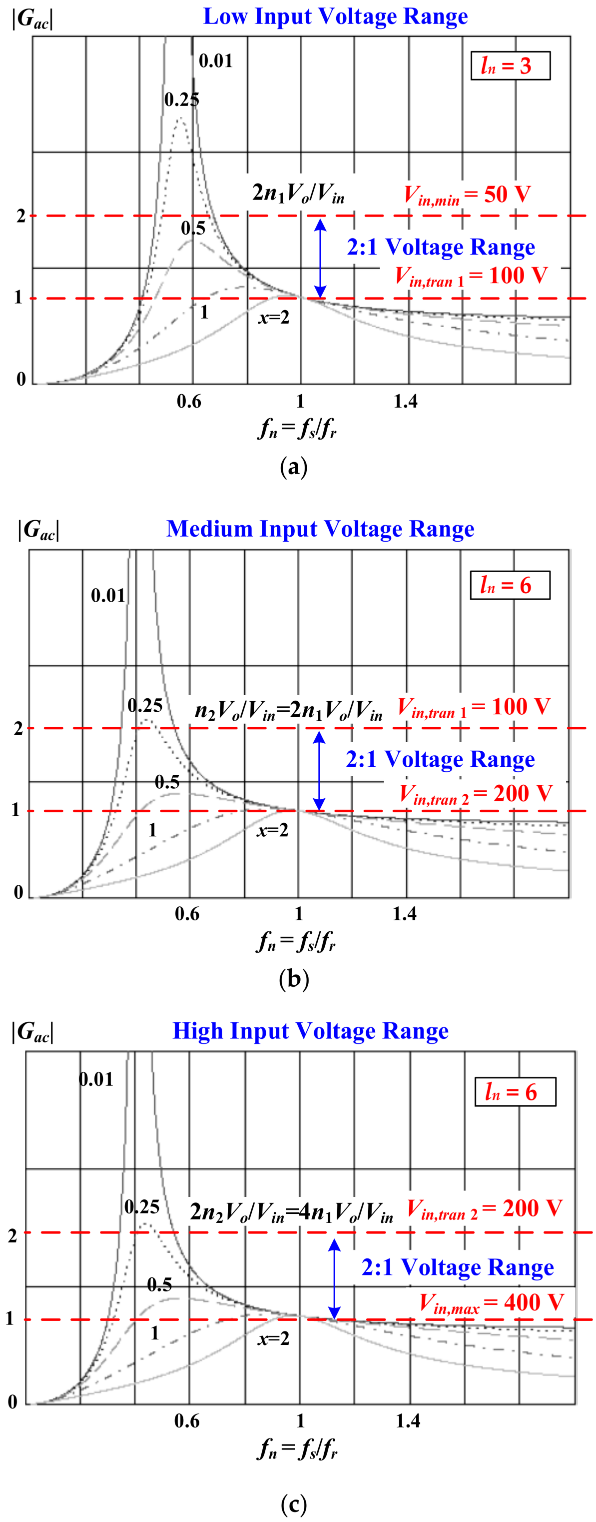

Figure 7. Voltage curves of the presented circuit: (**a**) low input voltage range; (**b**) medium input voltage range; (**c**) high input voltage range.

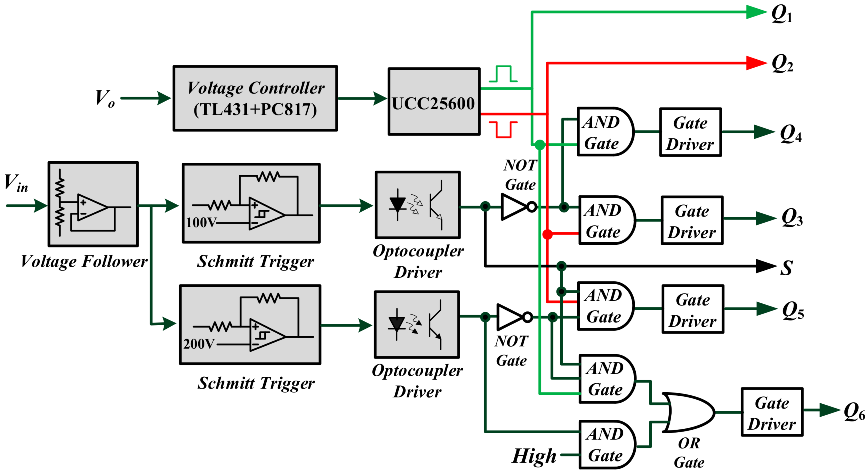

Figure 8. Control block of the signals Q_1–Q_6 and S.

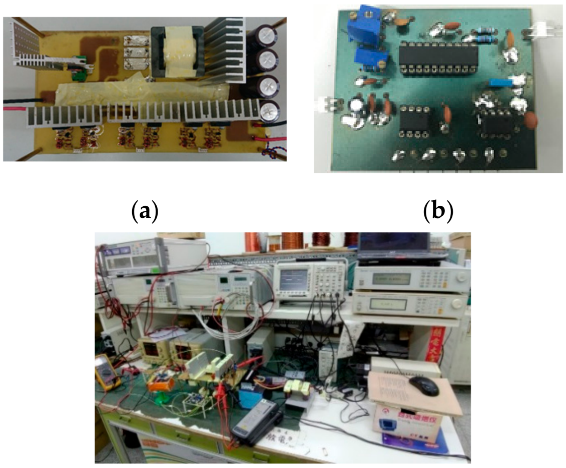

(**a**) (**b**)

(**c**)

Figure 9. Pictures of the proposed converter: (**a**) prototype circuit; (**b**) control board; (**c**) experimental setup.

Table 1. Prototype circuit parameters.

Items	Symbol	Parameter
Input voltage	V_{in}	50–400 V
Output voltage	V_o	48 V
Rated load current	I_o	10 A
Series resonant frequency	f_r	150 kHz
Output capacitor	C_o	1080 µF (1080 µF/100 V)
Resonant capacitors	C_{r1}, C_{r2}	273 nF
Power MOSFETs	Q_1–Q_6, S	Infineon-6R070P6
Resonant inductors	L_{r1}, L_{r2}	4.13 µH
Rectifier diodes	D_1, D_2	PS30M100SFP
Primary and secondary turns of T	n_p, n_s	8 turns, 4 turns

The experimental waveforms of the developed circuit operated at low input voltage range (V_{in} = 50–100 V) are shown in Figures 10 and 11. In the low input voltage range, power switches S, Q_5, and Q_6 were off and only switches Q_1–Q_4 were controlled with frequency modulation. Figure 10 illustrates the experimental results at V_{in} = 50 V input and full load. Figure 10a gives the test waveforms of $v_{Q1,g}$–$v_{Q4,g}$. The switching frequency f_{sw} under the rated power and V_{in} = 50 V was about 100 kHz.

Figure 10b provides the test waveforms of primary-side current i_{Lr1}, capacitor voltage v_{Cr1}, and leg voltage v_{ab}. Due to the switching frequency f_{sw} = 100 kHz < f_r = 150 kHz, the resonant current i_{Lr1} was a quasi-resonant waveform. Figure 10c shows the experimental waveforms of V_o, I_o, i_{D1}, and i_{D2}. One can observe that the output voltage was regulated at 48 V output, the load current I_o was 10 A, and the diodes D_1 and D_2 turned off at zero current switching. Figure 11 gives the experimental results at the rated power and V_{in} = 95 V. The measured gate voltages $v_{Q1,g}$–$v_{Q4,g}$ are given in Figure 11a. The test results of v_{ab}, v_{Cr1}, and i_{Lr1} are illustrated in Figure 11b. Because the switching frequency f_{sw} at V_{in} = 95 V was almost equal to f_r, the measured resonant inductor current i_{Lr1} was a sinusoidal waveform. The experimental waveforms of V_o, I_o, i_{D1}, and i_{D2} at the rated power and V_{in} = 95 V are demonstrated in Figure 11c. V_o was regulated well at 48 V output under I_o = 10 A. Figures 12 and 13 give the test results under the medium input voltage range (V_{in} = 100–200 V). Under the medium input voltage range, switches Q_3 and Q_4 were off and S was on. Figure 12 shows the test results under V_{in} = 105 V and full load. Figure 12a gives the measured gate voltages $v_{Q1,g}$, $v_{Q2,g}$, $v_{Q5,g}$, and $v_{Q6,g}$. The measured switching frequency f_{sw} was about 84 kHz. Figure 12b provides the test results of v_{Cr1}, i_{Lr1}, v_{Cr2}, and i_{Lr2}. Because f_{sw} = 84 kHz < f_r = 150 kHz, the resonant currents i_{Lr1} and i_{Lr2} were the quasi-sinusoidal waveforms. Figure 12c provides the measured waveforms of V_o, I_o, i_{D1}, and i_{D2} at the rated power and V_{in} = 105 V. The diodes D_1 and D_2 turned off at zero current switching. Similarly, the measured waveforms of the proposed converter under V_{in} = 195 V and full load are provided in Figure 13. The measured switching frequency f_{sw} = 163 kHz at V_{in} = 195 V and full load so that i_{Lr1} and i_{Lr2} were the sinusoidal waveforms, as shown in Figure 13b. Under the high input voltage range (V_{in} = 200–400 V), power switches Q_3, Q_4, and Q_5 were off, and S and Q_6 were on. Figure 14 shows the experimental waveforms under V_{in} = 205 V, V_o = 48 V, and P_o = 480 W. Figure 14a shows the measured gate voltages $v_{Q1,g}$, $v_{Q2,g}$, $v_{S,g}$, and $v_{Q6,g}$. The measured switching frequency f_{sw} = 82 kHz at V_{in} = 205 V. Figure 14b provides the measured waveforms i_{Lr1}, i_{Lr2}, v_{Cr1}, and v_{Cr2}. Due to f_{sw} (82 kHz) < f_r (150 kHz), the measured currents i_{Lr1} and i_{Lr2} were the quasi-sinusoidal waveforms. Figure 14c gives the measured waveforms V_o, I_o, i_{D1}, and i_{D2}. The diodes D_1 and D_2 turned off at zero current with soft switching operation. Figure 15 provides the experimental waveforms at the rated power and V_{in} = 400 V. The switching frequency f_{sw} = 160 kHz. The measured switch waveforms of Q_1 at V_{in} = 50, 95, 195, and 400 V cases are measured in Figure 16. One can observe that Q_1 all turned on at zero voltage switching. It can be predicted that Q_2–Q_6 were also turned on under zero voltage due to the *LLC* (inductor-inductor-capacitor) series resonant behavior. Figure 17 provides the measured circuit efficiencies for different load power (20%, 50%, and 100% loads) and input voltages (V_{in} = 50–400 V). For the same output power, the primary-side current at low input voltage range such as V_{in} = 50 V was greater than high input voltage range such as V_{in} = 205 V. This will introduce more conduction losses on the primary-side components under low input voltage range. Therefore, the presented circuit had better circuit efficiency at the high input voltage range.

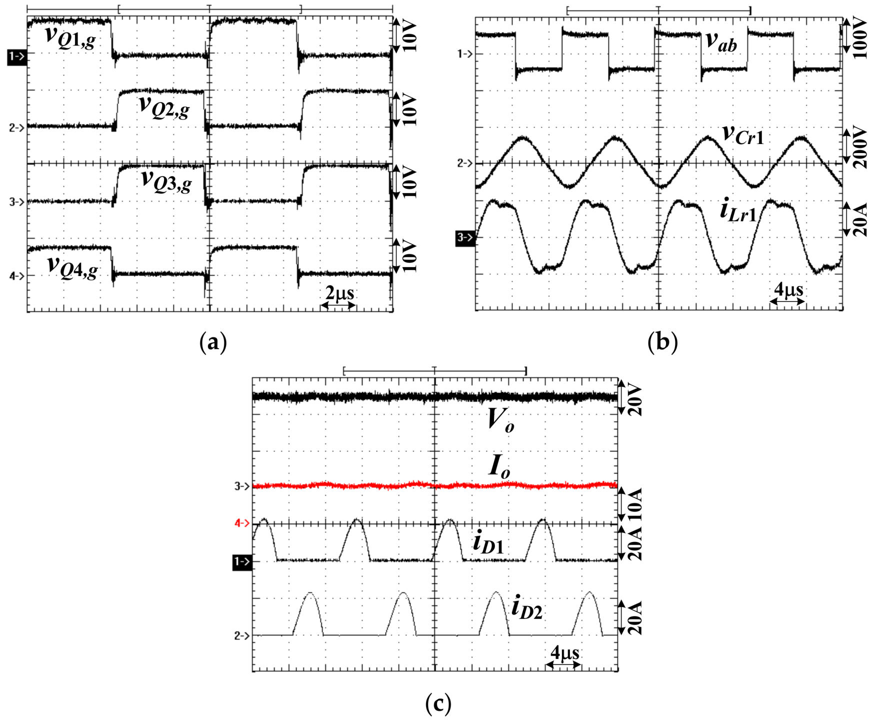

Figure 10. Experimental results at V_{in} = 50 V and full load: (**a**) $v_{Q1,g}$~$v_{Q4,g}$; (**b**) v_{ab}, v_{Cr1}, i_{Lr1}; (**c**) V_o, I_o, i_{D1}, i_{D2}.

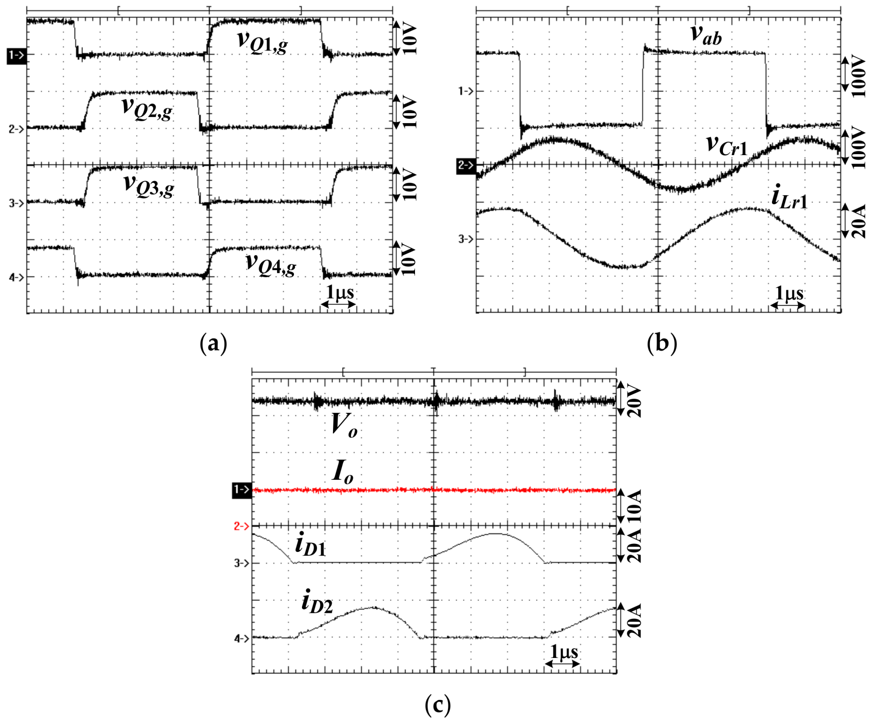

Figure 11. Experimental results at V_{in} = 95 V and full load: (**a**) $v_{Q1,g}$~$v_{Q4,g}$; (**b**) v_{ab}, v_{Cr1}, i_{Lr1}; (**c**) V_o, I_o, i_{D1}, i_{D2}.

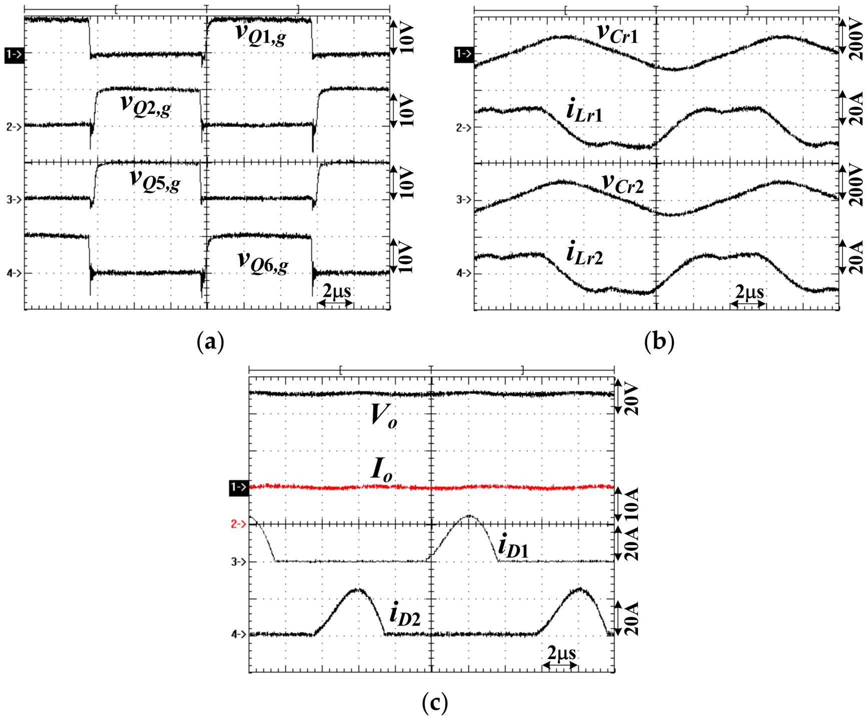

Figure 12. Experimental results at V_{in} = 105 V and full load: (**a**) $v_{Q1,g}$, $v_{Q2,g}$, $v_{Q5,g}$, $v_{Q6,g}$; (**b**) v_{Cr1}, i_{Lr1}, v_{Cr2}, i_{Lr2}; (**c**) V_o, I_o, i_{D1}, i_{D2}.

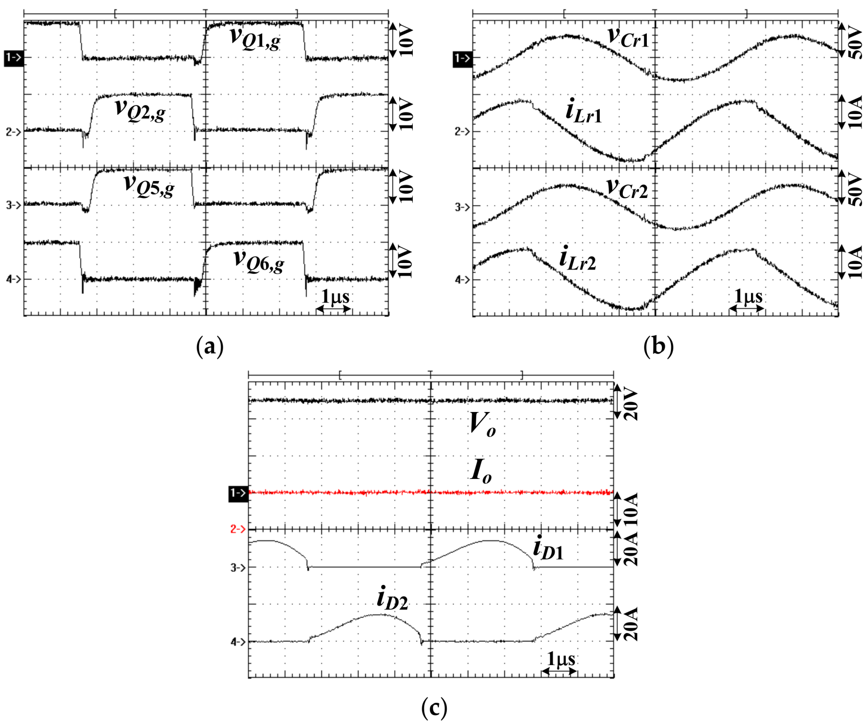

Figure 13. Experimental results at V_{in} = 195 V and full load: (**a**) $v_{Q1,g}$, $v_{Q2,g}$, $v_{Q5,g}$, $v_{Q6,g}$; (**b**) v_{Cr1}, i_{Lr1}, v_{Cr2}, i_{Lr2}; (**c**) V_o, I_o, i_{D1}, i_{D2}.

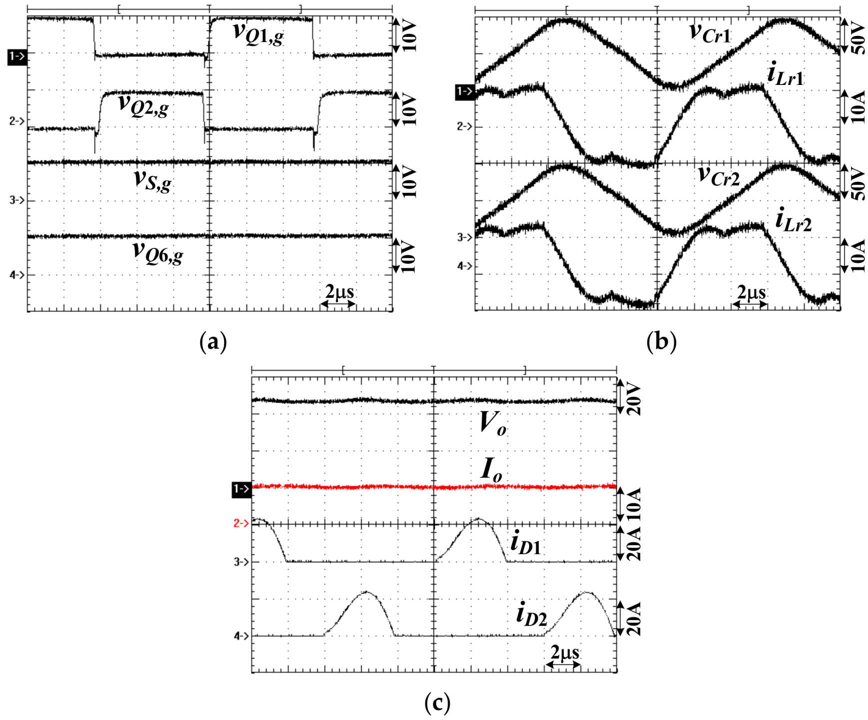

Figure 14. Experimental results at V_{in} = 205 V and full load: (**a**) $v_{Q1,g}$, $v_{Q2,g}$, $v_{S,g}$, $v_{Q6,g}$; (**b**) v_{Cr1}, i_{Lr1}, v_{Cr2}, i_{Lr2}; (**c**) V_o, I_o, i_{D1}, i_{D2}.

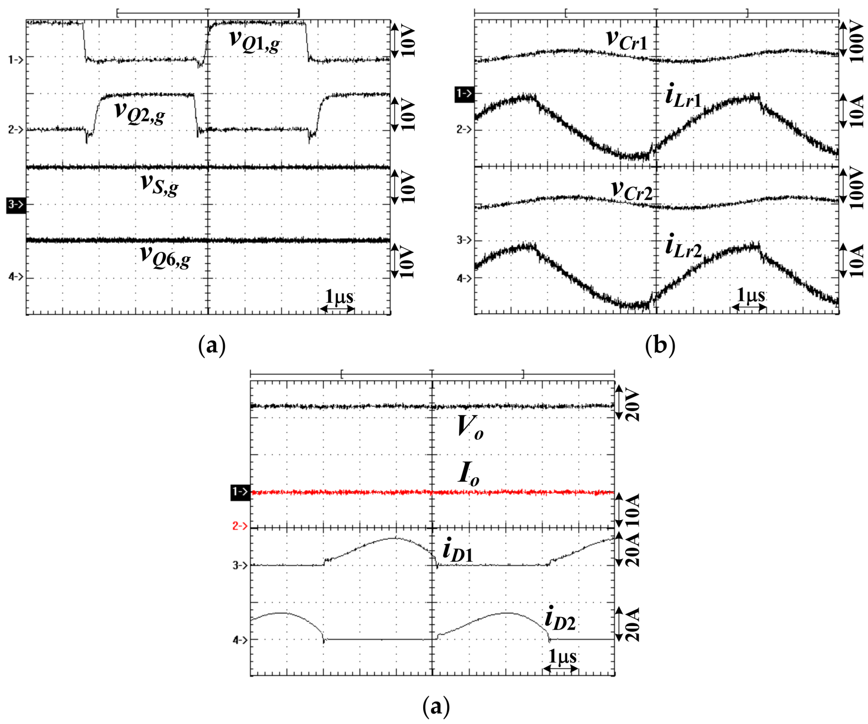

Figure 15. Experimental results at V_{in} = 400 V and full load: (**a**) $v_{Q1,g}$, $v_{Q2,g}$, $v_{S,g}$, $v_{Q6,g}$; (**b**) v_{Cr1}, i_{Lr1}, v_{Cr2}, i_{Lr2}; (**c**) V_o, I_o, i_{D1}, i_{D2}.

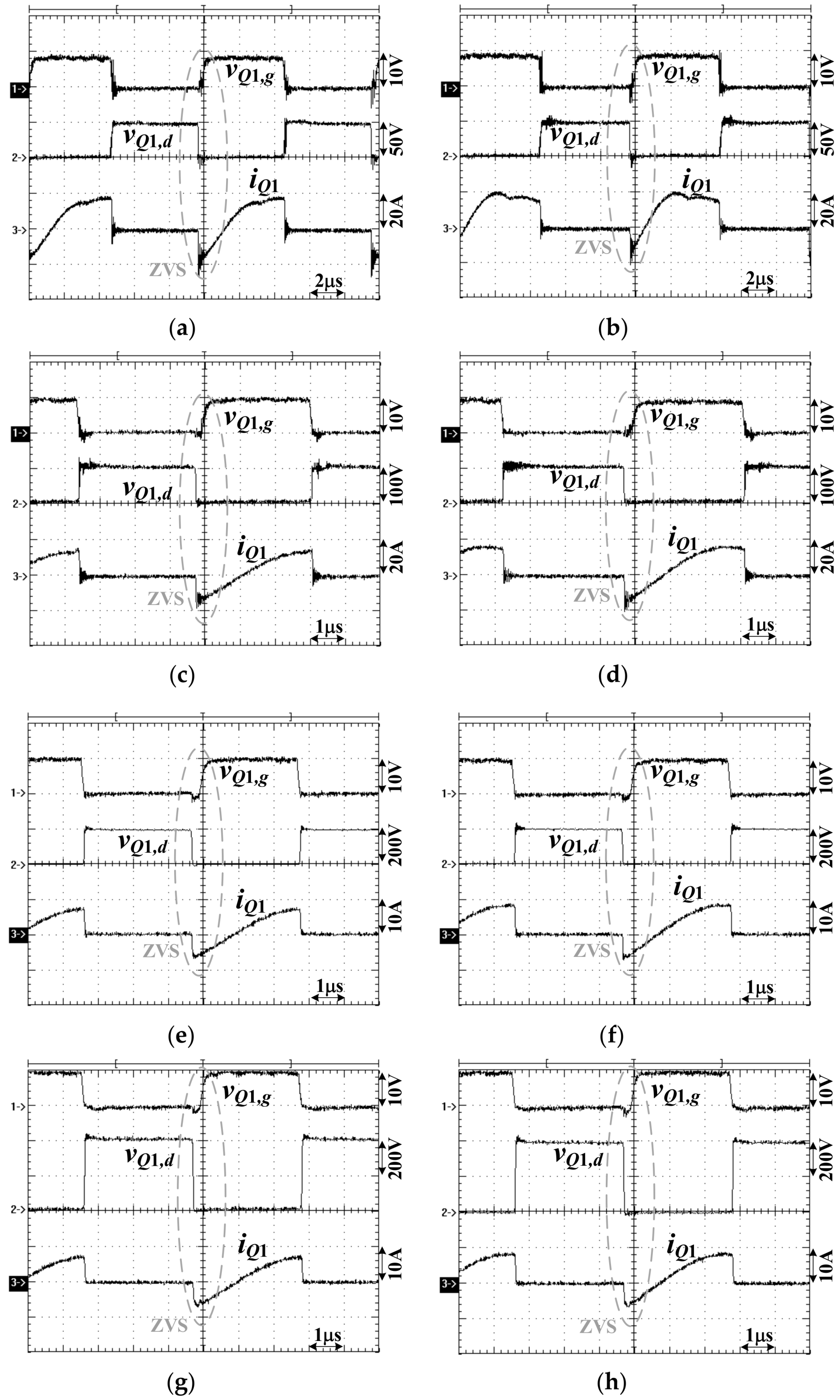

Figure 16. Experimental results at switch Q_1 under (**a**) V_{in} = 50 V and 50% load; (**b**) V_{in} = 50 V and 100% load; (**c**) V_{in} = 95 V and 50% load; (**d**) V_{in} = 95 V and 100% load; (**e**) V_{in} = 195 V and 50% load; (**f**) V_{in} = 195 V and 100% load; (**g**) V_{in} = 400 V and 50% load; (**h**) V_{in} = 400 V and 100% load.

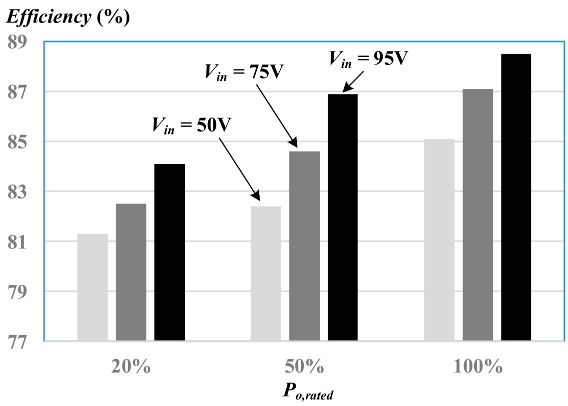

(**a**)

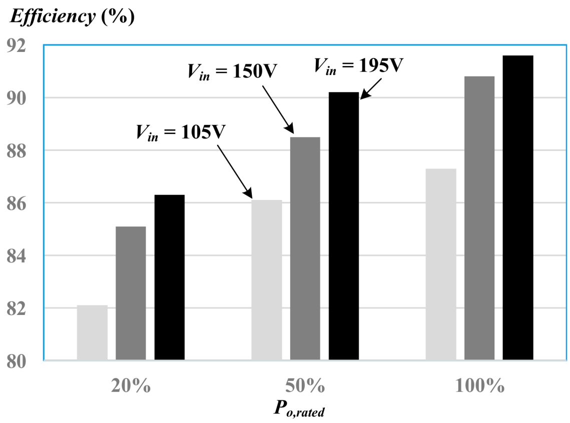

(**b**)

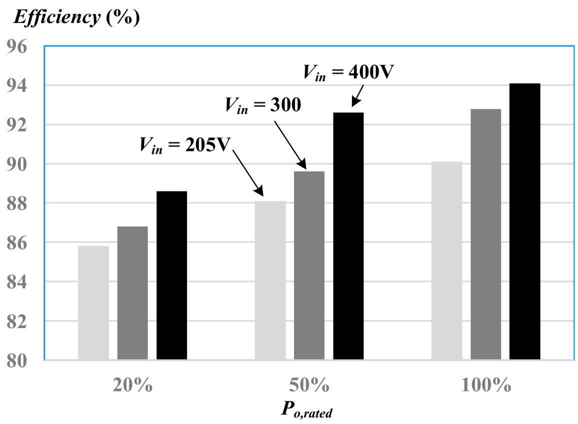

(**c**)

Figure 17. Measured circuit efficiencies: (**a**) low input voltage range; (**b**) medium input voltage; (**c**) high input voltage range.

5. Conclusions

The main contribution of the proposed converter is wide voltage operation capability compared to the conventional single-stage or two-stage converters. In conventional single-stage or two-stage PWM converters or resonant converters, the input voltage variation range is normally less than a 4:1 voltage range. The presented circuit has three equivalent operation circuits with half bridge to full bridge circuit topology to change the voltage gain between the output and input voltages. Each equivalent resonant circuit can achieve a 2:1 input voltage operation range, that is, $V_{in,max} = 2V_{in,min}$. Therefore, three equivalent resonant circuits can achieve an 8:1 wide input voltage range operation, that is, $V_{in,max}$ = $8V_{in,min}$. For the low input voltage range, the full-bridge resonant converter with low turns ratio of transformer is operated to obtain the higher voltage gain between the load voltage and input voltage. For the medium input voltage range, the other full bridge resonant circuit topology with high turns ratio is selected to obtain the lower voltage gain. The half bridge resonant converter is selected to achieve the lowest voltage gain under the high input voltage range. Therefore, the presented converter with three equivalent sub-circuits can accomplish an 8:1 wide input voltage operation. Due to resonant circuit characteristics, the power switches can have soft switching operation over wide range of load conditions. Three equivalent sub-circuits are selected according to the input voltage range with two Schmitt comparators. The applications of the presented resonant circuit can be the front stage of solar power conversion with wide input voltage variation. The theoretical converter characteristics were confirmed by the measured waveforms from a laboratory circuit. The measured results confirmed the converter performance with wide voltage range operation. The further works of this project are to increase the circuit efficiency by using the synchronous rectifiers on the output side and designing the isolated transformer with minimum core and copper losses.

Author Contributions: B.-R.L. proposed and designed this project and wrote this paper. Y.-S.Z. measured the circuit waveforms in the experiment. All authors have read and agreed to the published version of the manuscript.

Funding: This research is funded by the Ministry of Science and Technology, Taiwan, under grant number MOST 108-2221-E-224-022-MY2.

Acknowledgments: This research is funded by the Ministry of Science and Technology, Taiwan, under grant number MOST 108-2221-E-224-022-MY2.

Conflicts of Interest: The authors declare no potential conflict of interest.

References

1. Liu, P.J.; Hsu, Y.C.; Hsu, S.R. Drain-voltage balance and phase-shifted PWM control schemes for high-efficiency parallel-string dimmable LED drivers. *IEEE Trans. Ind. Electron.* **2018**, *65*, 6168–6176. [CrossRef]
2. Safaee, A.; Jain, P.; Bakhshai, A. A ZVS pulsewidth modulation full-bridge converter with a low-RMS-current resonant auxiliary circuit. *IEEE Trans. Power Electron.* **2016**, *31*, 4031–4047. [CrossRef]
3. Wang, Y.; Zhang, S.; Guan, Y.; Liu, X.; Xu, D. Single-stage QR ac-dc converter based on buck-boost and flyback circuits. *IET Power Electron.* **2017**, *10*, 103–111. [CrossRef]
4. Xie, X.; Li, J.; Peng, K.; Zhao, C.; Lu, Q. Study on the single-stage forward-flyback PFC converter with QR control. *IEEE Trans. Power Electron.* **2016**, *31*, 430–442. [CrossRef]
5. Lin, B.R.; Chiang, H.K.; Chen, C.C. Analysis and implementation of a zvs-pwm converter with series-connected transformers. *IEEE Trans. Circuits Syst. II* **2007**, *54*, 917–921. [CrossRef]
6. Lin, B.R.; Lin, Y. Parallel current-fed resonant converter with balance current sharing and no input ripple current. *IET Power Electron.* **2019**, *12*, 212–219. [CrossRef]
7. Haga, H.; Kurokawa, F. Modulation method of a full-bridge three-level LLC resonant converter for battery charger of electric vehicles. *IEEE Trans. Power Electron.* **2017**, *32*, 2498–2507. [CrossRef]
8. Zhang, Y.; Fu, C.; Sumner, M.; Wang, P. A wide input-voltage range quasi-Z-source boost DC–DC converter with high-voltage gain for fuel cell vehicles. *IEEE Trans. Ind. Electron.* **2018**, *65*, 5201–5212. [CrossRef]
9. Yao, Z.; Xu, J. A three-phase DC-DC converter for low and wide input-voltage range application. In Proceedings of the 2016 IEEE Transportation Electrification Conference and Expo, Asia-Pacific (ITEC Asia-Pacific), Busan, Korea, 1–4 June 2016; pp. 208–213.
10. Li, W.; Zong, S.; Liu, F.; Yang, H.; He, X.; Wu, B. Secondary-side phase-shift-controlled ZVS DC/DC converter with wide voltage gain for high input voltage applications. *IEEE Trans. Power Electron.* **2013**, *28*, 5128–5139. [CrossRef]
11. Lu, J.; Kumar, A.; Afridi, K.K. Step-down impedance control network resonant DC-DC converter utilizing an enhanced phase-shift control for wide-input-range operation. *IEEE Trans. Ind. Appl.* **2018**, *54*, 4523–4536. [CrossRef]

12. Wu, H.; Wan, C.; Sun, K.; Xing, Y. A high step-down multiple output converter with wide input voltage range based on quasi two-stage architecture and dual-output *LLC* resonant converter. *IEEE Trans. Power Electron.* **2015**, *30*, 1793–1796. [CrossRef]
13. Hu, H.; Fang, X.; Chen, F.; Shen, Z.J.; Batarseh, I. A modified high-efficiency LLC converter with two transformers for wide input-voltage range applications. *IEEE Trans. Power Electron.* **2012**, *28*, 1946–1960. [CrossRef]
14. Shang, C.; Liu, L.; Liu, M.; Men, S. A highly-efficient two-stage DC-DC converter with wide input voltage. In Proceedings of the 2015 IEEE International Telecommunications Energy Conference (INTELEC), Osaka, Japan, 18–22 October 2015; pp. 1–6.
15. Zhou, G.; Ruan, X.; Wang, X. Input voltage feed-forward control strategy for cascaded DC/DC converters with wide input voltage range. In Proceedings of the 2016 IEEE 8th International Power Electronics and Motion Control Conference (IPEMC-ECCE Asia), Hefei, China, 22–26 May 2016; pp. 603–608.
16. Jeong, Y.; Kim, J.K.; Lee, J.B.; Moon, G.W. An asymmetric half-bridge resonant converter having a reduced conduction loss for DC/DC power applications with a wide range of low input voltage. *IEEE Trans. Power Electron.* **2017**, *32*, 7795–7804. [CrossRef]
17. Wang, P.; Zhou, L.; Zhang, Y.; Li, J.; Sumner, M. Input-parallel output-series DC-DC boost converter with a wide input voltage range, for fuel cell vehicles. *IEEE Trans. Veh. Technol.* **2017**, *66*, 7771–7781. [CrossRef]
18. Kim, B.; Kim, S.; Huh, D.Y.; Choi, J.H.; Kim, M. Hybrid resonant half-bridge DC/DC converter with wide input voltage range. In Proceedings of the 2018 IEEE Applied Power Electronics Conference and Exposition (APEC), San Antonio, TX, USA, 4–8 March 2018; pp. 1876–1881.
19. Singh, A.K.; Das, P.; Panda, S.K. Analysis and design of SQR-based high-voltage LLC resonant dc-dc converter. *IEEE Trans. Power Electron.* **2017**, *32*, 4466–4481. [CrossRef]
20. Sun, W.; Xing, Y.; Wu, H.; Ding, J. Modified high-efficiency LLC converters with two split resonant branches for wide input-voltage range applications. *IEEE Trans. Power Electron.* **2018**, *33*, 7867–7870. [CrossRef]
21. Jovanović, M.M.; Irving, B.T. On the fly topology-morphing control efficiency optimization method for LLC resonant converters operating in wide input and/or output-voltage range. *IEEE Trans. Power Electron.* **2016**, *31*, 2596–2608. [CrossRef]
22. Steigerwald, R.L. A comparison of half-bridge resonant converter topologies. *IEEE Trans. Power Electron.* **1988**, *3*, 174–182. [CrossRef]